Available online at www.sciencedirect.com
SCIENCE DIRECT®
Neurocomputing 69 (2006) 1599–1607
NEUROCOMPUTING
www.elsevier.com/locate/neucom

Speed estimation with propagation maps

C. Rasche*

Department of Psychology, University of Notre Dame, Notre Dame, IN, USA

Received 13 January 2004; received in revised form 19 March 2005; accepted 25 May 2005
Available online 25 October 2005
Communicated by T. Heskes

Abstract

We propose a neural architecture that estimates the speed of motion. The basis is a two-dimensional map made of locally connected integrate-and-fire neurons, that propagates and integrates synaptic input in a dendritic-cable-like manner, but irrespective of any direction. The propagation dynamics of such a map are tuned to filter preferred speeds: slow map dynamics filter slow speeds, fast map dynamics filter fast speeds. The propagation map is potentially simple enough for an analog hardware approach.

Keywords: Motion detection; Speed estimation; Wave propagation; Propagation map

1. Introduction

Biophysical models of motion detection generally aim at explaining the mechanism for direction selectivity. One line of models pursues to explain direction selectivity by the sequential stimulation of excitatory and inhibitory synapses, whose spatial input order corresponds to the preferred stimulus direction. For example, if an excitatory synapse is stimulated first, followed by an inhibitory synaptic stimulation, the cell fires because the delayed inhibitory stimulation was not able to block the excitatory input. Stimulation in the opposite direction in turn would trigger inhibition first, which would block a following excitatory input. Such synaptic interplays can be summarized as synaptic logic [12] and may be employed by biological visual systems to compute direction selectivity in insects [22] and vertebrate [1] in one way or the other. A variant of this delay-and-compare scheme is synaptic integration in a dendritic branch [17]: if synaptic input is subsequently placed along a dendritic cable towards the soma, it will result in a gradually increasing wave that reaches the spiking threshold in the soma. Placement of synaptic input into the opposite direction—away from the soma—does not cause spiking. Such dendritic integration may also be employed by the nervous system (e.g. [13]). Less effort has been invested into inventing biophysical models that estimate the speed of object motion.

An alternative system was suggested by Glaser and Barch, who model motion detection on a map level [9]. They introduced the idea of an excitable neuronal array in which neurons are locally connected. When such a map is stimulated with a motion stimulus it leaves behind a characteristic wave propagation pattern. Some of these propagation patterns can explain certain types of motion illusions. In such maps, a motion of the same direction but different speed triggers different propagation patterns. What this line of studies has not addressed yet, is how direction and speed can be explicitly represented and read out in a simple neuronal way: what would be the specific mechanism that could distinguish between two directions or two speeds? We address this question here for the issue of speed estimation only. Our intuition is that one can obtain different speed estimates by using multiple maps with different dynamics, or more figurally speaking, maps with different viscosity. Fast map dynamics (short-time constants) would be used for detecting high speeds, slow map dynamics (long-time constants) would be used for low speeds. To signal the presence of a certain speed, the corresponding map would generate spikes. In other words, the combined firing of the entire map, the population signal, would signal the presence of a specific speed.

*Corresponding author. Present address: 417 Moore Building, Department of Psychology, The Pennsylvania State University, University Park, PA 16802, USA. Tel.: +1 814 865 1930; fax: +1 814 867 1107.
E-mail address: cur12@psu.edu.

0925-2312/$ - see front matter © 2005 Elsevier B.V. All rights reserved.
doi:10.1016/j.neucom.2005.05.013

Glaser and Barch's propagation map consists of 'continuous' neurons and does not possess the ability to deliver the envisioned population output. We therefore introduce a spiking propagation map, which we also have used in for other visual tasks [18,20]. Synaptic input placed into such a propagation map, will spread to all directions and decay in amplitude similar to the propagation properties of synaptic input in a dendritic cable. Sequential synaptic input along any direction will gradually integrate and eventually reach the spiking threshold and therefore cause spiking. In order to differentiate between various speeds, the map's dynamics are adjusted correspondingly to filter only a certain speed or range of speeds. An important advantage of such maps is, that speed estimation is independent of direction. That is, the tedious placement of direction-selective cables or the spatial arrangement of synapses falls away. Summarized roughly, these types of propagation maps embody Rall's delay-and-compare scheme but irrespective of motion direction.

The remainder of the study aims at confirming our intuition of the speed-detecting propagation map with a simple software simulation, whereby we take an engineering viewpoint. We imagine a system in which a silicon retina (e.g. [2,14]), provides the input to such propagation maps in form of pulses (presynaptic spikes). The neuronal dynamics of the propagation map are chosen such that they resemble dynamics of neuronal, analog hardware [4,14]. In the discussion section, biophysical evidence is cited that may point towards the existence of such propagation maps in cortex.

2. Methods

A propagation map is a two-dimensional sheet of neurons, each horizontally connecting to its eight neighbors (Fig. 1). A neuron is modeled as a leaky integrate-and-fire unit, consisting of a single capacitance integrating the charge delivered by its synaptic input or horizontal connections, a spike-generating mechanism with fixed voltage threshold triggering a spike, a switch resetting the membrane potential when a spike is occurring, and a leakage conductance [12]. Integrate-and-fire units have been implemented into aVLSI in various forms (e.g. [14]). Instead of simulating the current and voltage dynamics explicitly, we merely model one variable corresponding to the membrane potential, the voltage V, of the neuron. When synaptic input drives V above the spiking threshold, V is set to a maximum value, E_{Na}—interpreted as the reversal potential for sodium, shortly thereafter V is set to a minimum value, E_{K}—interpreted as the reversal potential for potassium. The synaptic input from a neighboring neuron is proportional to the voltage difference between the pre- and post-synaptic neuron and can be interpreted as a resistor or conductance. The leakage conductance is chosen to be fixed and can be implemented with a single transistor.

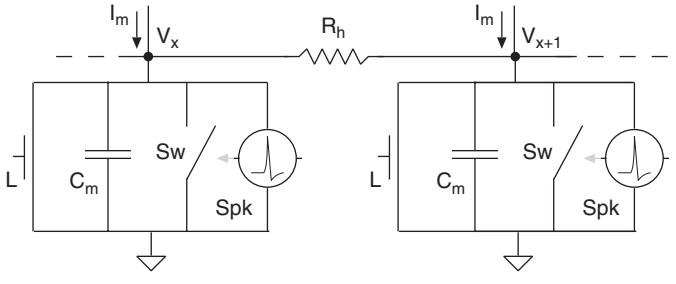

Fig. 1. Circuit diagram of the propagation map. Two connected units of integrate-and-fire type are shown. V_x ($V_{(x+1)}$): neuronal voltage. Cm: membrane capacitance. Sw: switch. Spk: spike generating mechanism. L: (constant) leakage conductance. R_{h}; horizontal resistance. I_{m}: external input (e.g. motion).

Below the spiking threshold the neuronal voltage is governed by the following equation. The neuronal voltage V at location (x, y), at its next step, $t+1$, is given by its present potential plus the input of its neighboring neurons via the horizontal connections, $I_{\mathrm{h}}(t)$, inhibitory input from its neighbors, $I_{\mathrm{i}}(t)$, external motion input, $I_{\mathrm{m}}(t)$, and a constant leakage L,

$$V(x,y,t+1) = V(x,y,t) + I_{\mathrm{h}}(t) - I_{\mathrm{i}}(t) - L + I_{\mathrm{m}}(t) \quad \text{for } V < V_{\mathrm{thres}};\ V = 0 \text{ for } V < 0. \tag{1}$$

I_{h} is the sum of positive membrane differences multiplied by the horizontal (or axial) conductance, $g_{\mathrm{h}} = (1/R_{\mathrm{h}})$, for each of its 8 neighboring neurons:

$$I_{\mathrm{h}}(t) = \sum_{k=1}^{8} \max[g_{\mathrm{h}}(V_k(t) - V(t)), 0], \tag{2}$$

where V_k is the voltage of the neighboring neurons. When V exceeds the spiking threshold, V_{thres}, a spike of duration d_{s} is triggered, followed by resetting V to ground (E_{K}). A horizontal resistor can be implemented in analog hardware in various ways, but in connection with a spiking unit, a switch-capacitor method is preferred [6,21]. The simulated dynamics of the present system are closest to a silicon dendrite implementation [21].

During a spike, a neuron will substantially contribute to its neighboring neurons and raise their activity level promptly. This may trigger rapidly growing, excessive spiking in the entire map. One could try to find the narrow parameter space in which that would not occur, but that would lead to intricate tuning. Rather, one introduces a stabilizing mechanism. We have chosen surround inhibition: when a neuron spikes it inhibits its neighboring neurons via inhibitory synapses. We express that as the neuron in question (Eq. (1)) receiving inhibitory input from its 8 neighbors whenever they spike:

$$I_{\mathrm{i}}(t) = \sum_{k=1}^{8} S_k(t) A_{\mathrm{i}}, \tag{3}$$

where $S_k(t)$ is the binarized spiking output of each neighboring neuron ($S(x,y,t) = [1 \text{ if } V(x,y,t) > V_{\text{thres}}, 0 \text{ otherwise}]$), A_i is the constant amplitude of the inhibitory synapse.

The external motion input, $I_m(t)$, consists of spikes, $S_m(t)$, multiplied by a synaptic amplitude A_e. Spikes are assumed to be triggered by motion-sensitive cells in a retina or maybe lower visual cortical area. A_e is the constant amplitude of the excitatory input synapse. During a motion stimulus, the activated synapses are stimulated only once (sequentially) and we sometimes refer to the resulting postsynaptic responses as EPSP drops. The dynamics of any postsynaptic response—whether A_i or A_e—is chosen to be merely pulse-shaped with a duration of one time step.

We have chosen some parameter values in accordance to voltage values in analog VLSI circuits for reason of familiarity [5], but the values possess no specific unit. E_{Na} and E_K are set to 5 and 0, respectively. The spiking threshold is set to be 2.0. The simulation time step is 0.2 and can be interpreted as milliseconds. The spike duration lasts one time step (a value of 0.2).

Ten speeds were use to test the propagation map: 0.03 (slowest) to 0.3 (fastest) in steps of 0.03. The corresponding time intervals are $33.3, 16.6, \ldots, 3.7$ and 3.3 (1/speed in simulation units). Five different parameter sets were created to demonstrate the speed-selective characteristics of the maps, whose dynamics range from 'very fast', detecting only very fast motion stimulation, down to 'very slow', detecting only very slow motion stimulation:

$g_h = 0.80;\ L = 0.25;\ A_i = 2.2;\ A_e = 0.5$ (very fast),
$g_h = 0.50;\ L = 0.20;\ A_i = 1.5;\ A_e = 0.5$ (fast),
$g_h = 0.12;\ L = 0.08;\ A_i = 0.0;\ A_e = 0.6$ (medium),
$g_h = 0.05;\ L = 0.01;\ A_i = 0.7;\ A_e = 0.6$ (slow),
$g_h = 0.02;\ L = 0.01;\ A_i = 0.6;\ A_e = 0.7$ (very slow).

The parameter values were found as follows. Firstly, we determined two extreme dynamics, 'very fast' versus 'very slow', which caused spiking only for the extreme speeds, number 1 and 10, respectively. The intermediate dynamics (fast, medium and slow) were then intuitively interpolated requiring only little tuning effort (a few trials). The tuning of the g_h and L values is explained in the 1st paragraph of the result section. The value A_i was found by increasing it until it would prevent excessive spiking for all speeds. A_i is higher for faster maps because they can easier derail due to their swift dynamics. The value for the medium map is 0, because we have accidentally found a stable parameter space, in which surround inhibition is not required. The value for A_e was adjusted such, that it would trigger spiking with at least the 10th EPSP drop for a preferred speed. A_e is required to be higher for slower maps, otherwise the spiking threshold would never be reached for the given other parameters.

Speed is then signaled as follows: an approximate speed is signaled by the presence of spikes in a certain map. A specific speed is signaled by the number of spikes in the entire map across a certain period of stimulation.

3. Results

The map's propagation properties are analogous to the propagation properties of a dendritic cable disregarding the directionality of the cable. Changing the axial conductance, g_h, will primarily change the distance with which a signal spreads: a high value results in far spread, a low value in short spread, or put more formally, a high- and low-space constant, respectively. Changing the axial conductance also affects the decay time constant but to a smaller extent though: a high value causes a faster decay of activity at a given neuronal unit, whereas a low value causes a slower decay. Changing the amount of leakage, L, will primarily modulate the decay time constant: a low value results in a slow decay, whereas a high value results in a fast decay, or a long- and short-time constant, respectively. It will secondarily affect the space constant: a low leakage causes farther spread, a high leakage causes shorter spread. The detailed dynamics are highly non-linear due to the constant leakage term we have chosen, and are thus not quantitatively comparable to a perfect resistor-capacitor cable or map (see e.g. [14]).

In order to detect different speeds the above parameters are adjusted correspondingly. To detect fast speeds the axial conductance is set to a high value to allow for quick and far spread, resulting only in synaptic integration when there is a rapid sequence of EPSP drops. To avoid an integration of low speeds the leakage is set high. To detect slow speeds the reverse applies: a low value for the axial conductance avoids the fast run-away of activity and only slowly transmits activity to neighboring units. Additionally, the leakage conductance is set to a small value in order to give slow motion stimulation a chance to integrate.

We firstly examine the propagation and spiking characteristics of a 10×20 map in response to a moving dot stimulus. Fig. 2 visualizes the subthreshold propagation properties of two differently tuned maps. The dot wanders from left to right, from column number 2 to column number 17, at row number 5, triggering a single EPSP in each neuronal unit. The entire motion is shown in the upper left subplot of Fig. 2 as a line of stars. For an optimal stimulation the EPSPs gradually raise the subthreshold membrane potential, whose dynamics resemble an increasing, wandering mound. The upper two plots show the response of a dynamically fast map (parameter set 'very fast') in response to a fast-motion stimulation: the stimulation occurs at time steps $t = 1, 4, 9, 11$ and so on; the four plots show the map activity at time steps $t = 2, 5, 9$ and 12. The lower two plots show the response of a dynamically slow map (parameter set 'very slow') in response to a slow-motion stimulation: the stimulation occurs at time steps $t = 1, 34, 68, 101$ and so on; the four plots show the map activity at time steps $t = 2, 35, 69, 102$. In this case, the 4th stimulation leads already to a spike (see black dot in 'map'; the spike dynamics are cut off for the 'Xsect' diagram).

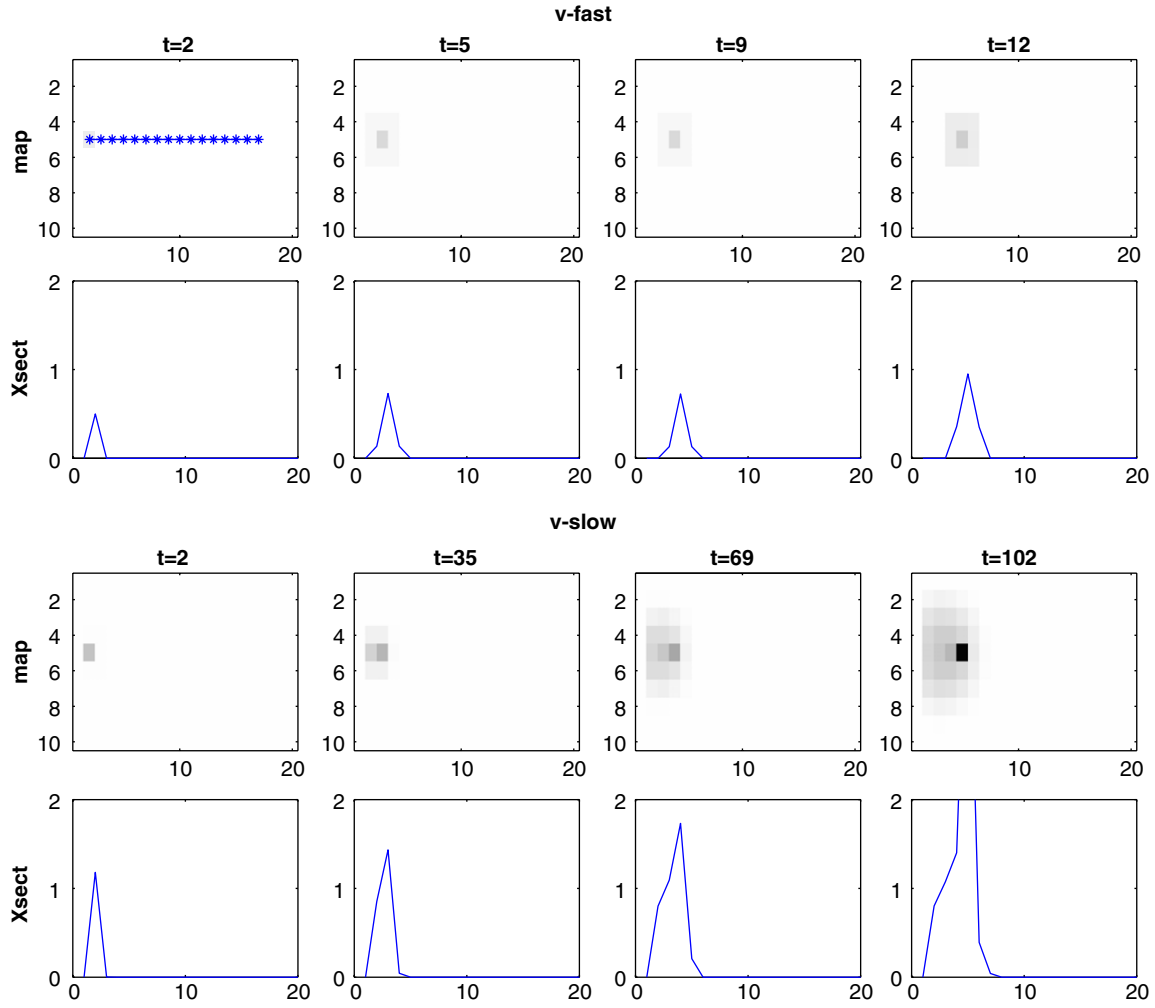

Fig. 2. Propagation properties of a map (10×20 neurons) in response to a moving dot [Y (row) $= 5$, X (column) $= 2, 3, \ldots, 17$, see stars in upper left subplot]. Upper two rows of plots: dynamically fast map, EPSP drops at $t = 1, 4, 9$ and 11 (speed number 10), map's response shown at $t = 2, 5, 9$ and 12. Lower two rows of plots: dynamically slow map, EPSP drops at $t = 1, 34, 68$ and 101 (speed number 1), map's response shown at $t = 2, 35, 69$ and 102. The map shows the subthreshold activity in gray-scale values. 'Xsect' shows a cross-section of the map at row number 5 (where stimulation occurs), only the subthreshold range (0..2) is shown.

Fig. 3 plots the spike occurrences for three differently tuned maps (fast, medium and slow) in response to different dot-stimuli speeds. The X-axis represents time in simulation units, the Y-axis represents the column coordinates of the spike occurrences (for row number 5). The motion stimulus is the same as before and is illustrated in this plot as a line connecting its EPSP drops. It starts at column number 2 and time step 1, and it ends at column number 17 and at a time unit that depends on the speed.

For the fast map, only speed numbers 8–10 caused spiking. Speed number 8 caused merely one spike after the 15th EPSP drop, which is marked with a single diamond. Speed number 9 triggered spiking after the 10th EPSP drop and then spiked 4 times with irregular intervals (4 diamonds connected by a line). For speed number 10 spiking started even earlier, namely after the 8th EPSP drop. For the medium map spiking occurred for speed numbers 4–8, with early onset of map spiking for speed number 5, and later onset for the other speeds. After onset of spiking spikes are triggered with every EPSP drop except for speed number 4. For the slow map speed numbers 1–6 caused spiking. Speed number 2 and 3 caused an early onset of map spiking. Spiking occurred only intermittent in comparison to the EPSP drops, which is partially due to a strong surround inhibition (high A_i).

A maps response was also tested with an arrow-shaped form, consisting of 5 dots pointing towards the right side (equivalent to a '>' sign). Fig. 4 shows spike plots, in which the map's spike occurrences are indicated by their gray-scale value, with bright and dark dots corresponding to early and late in time. No subthreshold activity is shown in this plot as opposed to the previous figure, which emphasized the subthreshold activity.

For the fast map there was only spiking for speed numbers 8–10, as there was for the dot stimulus. For the medium map however, there was spiking for more speeds (numbers 3–10) than for the dot stimulus, because the multiple EPSP drops of a shape add up. This has not such a

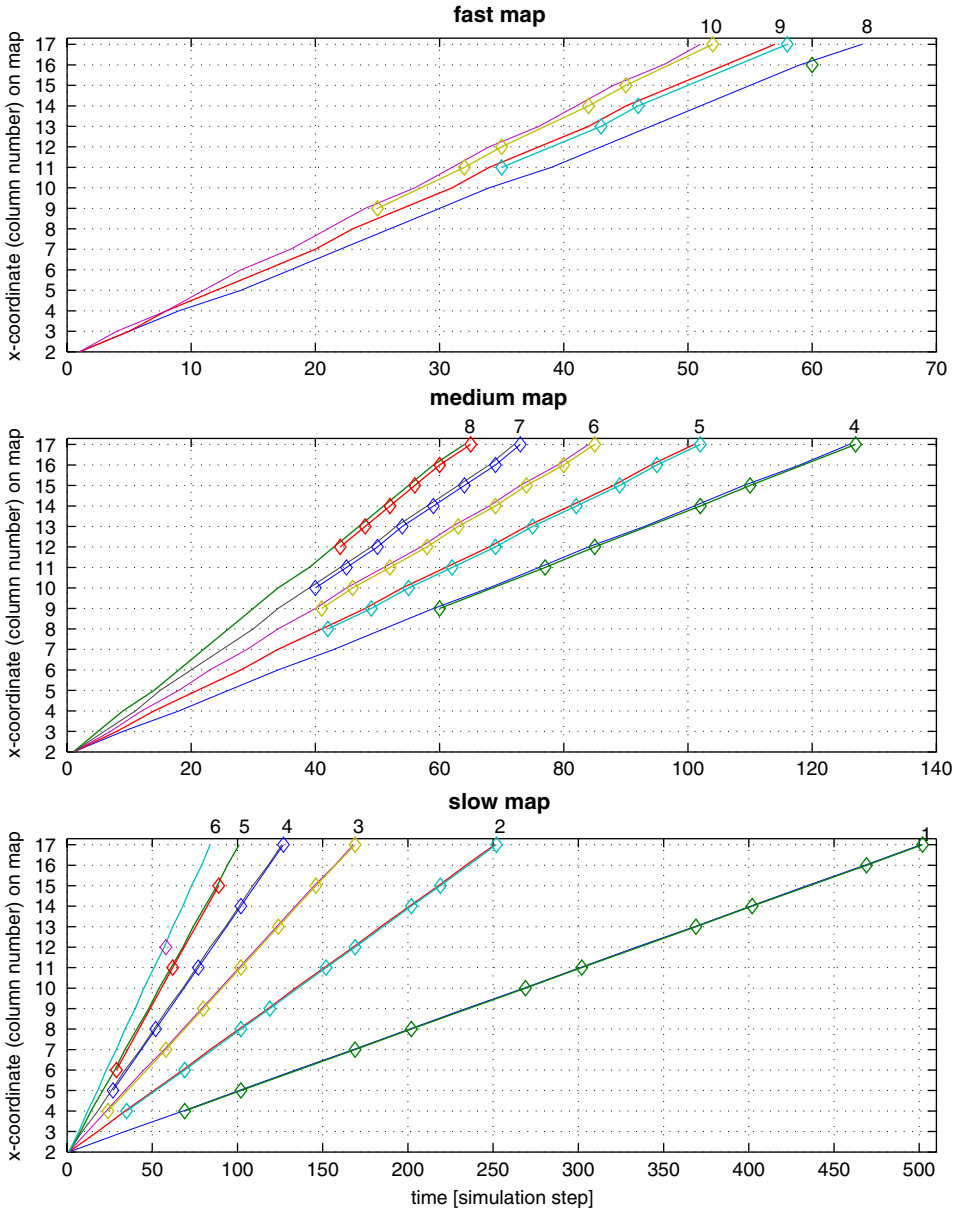

Fig. 3. Map spiking in response to the moving-dot stimulation for different speeds. *Y*-axis: *x*-coordinate (horizontal position) on propagation map. *X*-axis: time in simulation units. The input motion is described by a straight line. The map's spike occurrences are marked as diamonds connected by a line. Note that the time-axis scale for each map is different. Speed is detected and estimated by the presence and number of spikes, respectively. The plots visualize the gradual build up of activity, an increasing mound wandering to the right.

marked effect for the fast map, because the fast dynamics swallow the multiple EPSP drops easier. The response of the medium map to the fastest speed (number 10) does not actually reflect the shape form itself, but shows the summation from the neighboring shape dots sitting in the diagonal (each arrow 'wing' has three dots giving rise to two units receiving that type of summation). At lower speed it is the shape itself that determines the spike pattern. At medium speeds it is a mixture of both. For the slow map the map responded to every speed. At the highest, non-preferred speed the map spiked merely occasionally, at the slowest, preferred speed there was abundant spiking.

Fig. 5 shows the speed preference for each map for both motion stimulations, the dot and the arrow stimulation. The total number of spikes for an entire motion stimulus is plotted as a function of speed. We call these curves now speed-tuning curves. For the fast map both speed-tuning curves start at speed number 8 and increase with higher speeds. The curve of the arrow stimulation is higher due to the larger size of the stimulus. For the medium map the tuning curve for the dot starts at speed number 4 and ends at speed number 8 forming a bump. For the arrow stimulation the tuning curve covers a broader range of speeds, starting at speed number 3 and showing signs of decrease at speed numbers 9 and 10. For the slow map the

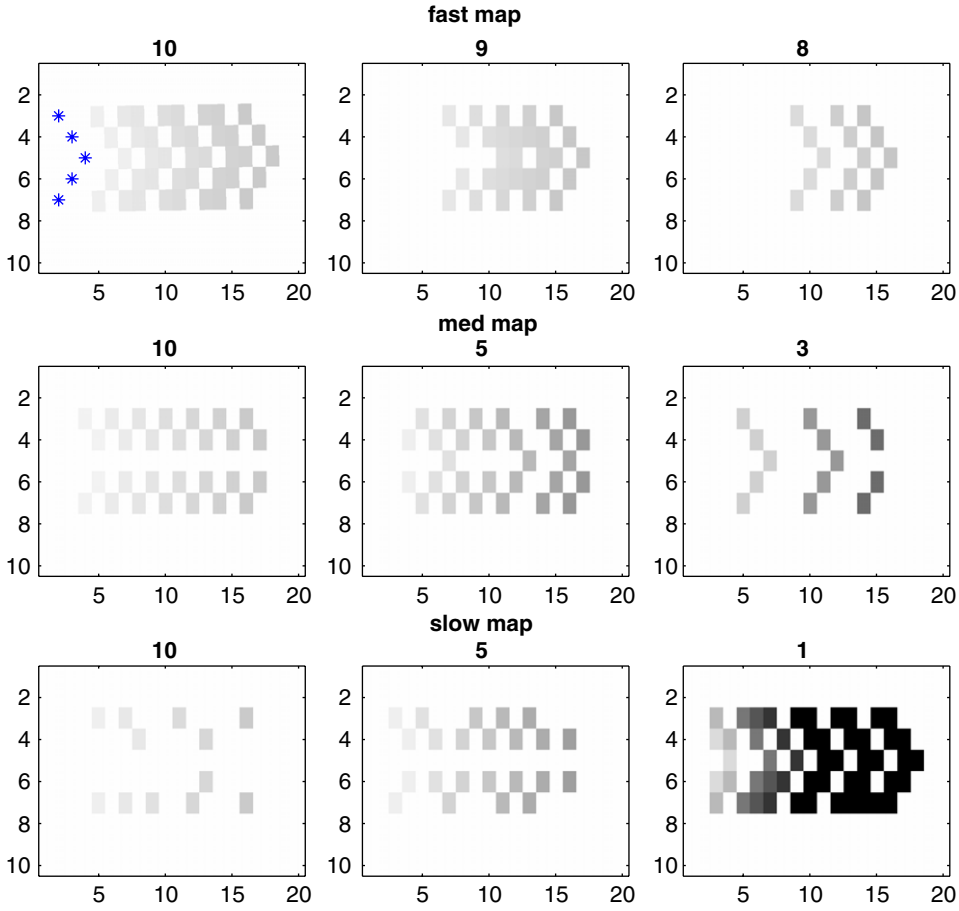

Fig. 4. Map spiking in response to a moving arrow shape (shape indicated in upper left subplot with asterisks) for three dynamically different maps (fast, medium and slow) and three different speeds. All spike occurrences are plotted into the map (10×20), with bright and dark dots representing early and late spiking, respectively (no subthreshold activity is shown). Fast map: response to speed numbers 10, 9 and 8 is shown. Medium map: response to speed numbers 10, 5 and 3 is shown. Slow map: response to speed numbers 10, 5 and 1 is shown. Reprinted with permission from Springer, Rasche 2005.

tuning curve for the dot covers the lower speeds (numbers 10–6) declining from low speeds to higher speeds, whereas the arrow stimulation covers the entire speed range, but also declining towards higher speeds. In summary, for the fast map one obtains a sharp tuning curve, which is less influenced by the number of input spikes (the shape size), for slower maps, the tuning curve broadens and does so even more when the shape size increases.

4. Discussion

The speed-tuning curves in Fig. 5 demonstrate that a propagation map captures a range of speeds, which is narrow for faster maps and broader for slower maps. Such curves thus allow only for a rough estimate of speed. In order to determine speed accurately, one could possibly use more maps and try to achieve a narrow tuning for each one, which however would likely result in a tuning ordeal. Yet, a better solution may be the employment of a pyramid that contained multiple layers with the same neuronal dynamics but receiving differently intermittent input from lower levels. A low level would receive input with small intervals and be sensitive to low speeds. Higher levels would receive only sparse input (large intervals) and therefore only detect high speeds. Such a 'speed-pyramid' would less depend on the need for different neuronal dynamics (see chapter 8 of [20] for a graphical illustration). In either case, the creation of a set of maps to cover all speeds is size-costly. Instead, it is more size efficient and even more accurate to create a set of neuron that read out a few tuning curves. For example, a neuron tuned for a specific speed, would read the ratio of firing rates from two or more maps, analogous to the formation of color sensation from only 3 photoreceptors with different luminance sensitivities. With such a neuronal readout, speeds could be determined much more accurately, despite the broad tuning-curves.

4.1. Steps towards an analog hardware approach

The purpose of the present study aimed at outlining an architecture that has the potential for an analog hardware implementation. As front-end, we envision a silicon retina that continuously generates pulses in response to any

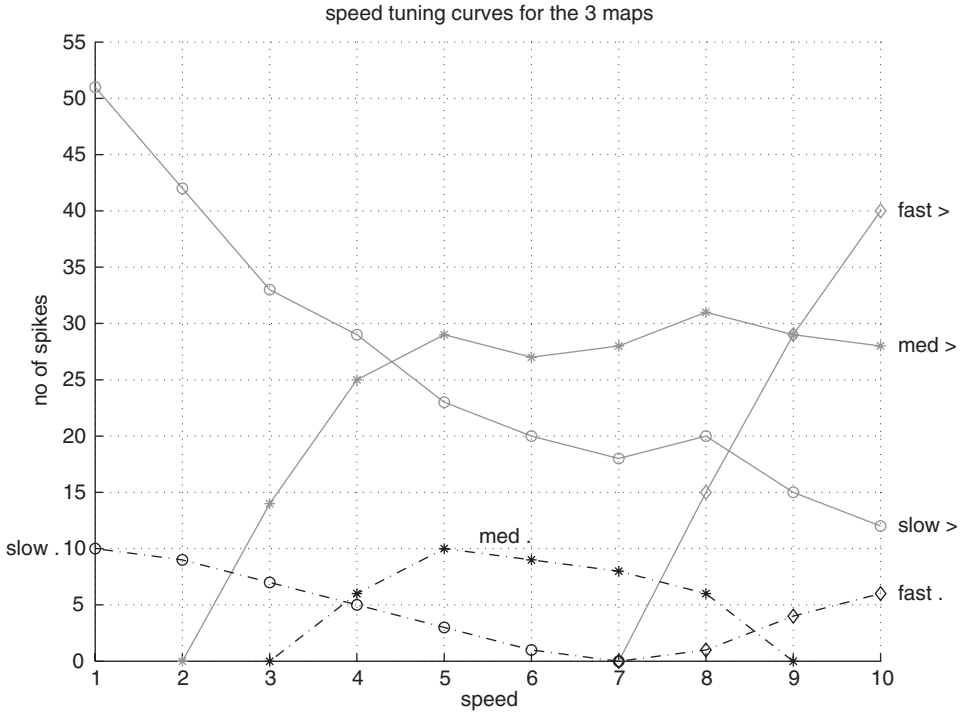

Fig. 5. Speed-tuning curves for each map (fast, medium, slow) for the dot (dashed–dotted lines) and arrow (solid lines) stimulation. *X*-axis: total number of occurred spikes for the entire stimulation, which represents the estimated speed. *Y*-axis: speed number. Reprinted with permission from Springer, Rasche 2005.

motion stimulus (e.g. [2,14]). These pulses would then be fed into the propagation maps. The silicon retina generates contours in response to motion stimulation by shapes. The simulation with the arrow (Fig. 4) was chosen to demonstrate that the propagation map also operates correctly with multiple, simultaneously appearing synaptic input that would derive from such contours.

To approach a transfer of the present architecture into analog hardware, it required firstly the proper design and analysis of the individual components, and then another round of software-simulations to determine the fine-tuning between the components. For the development of the suggested system the first step would be the construction of a propagation map. The present propagation map, with octagonal connectivity, is actually simulated with an Eq. (2) that emulates unidirectional flow of a resistor, because the octagonal connectivity with bidirectional resistors tends to generate unstable wave propagation [19]. It remains to be seen whether the presently simulated map could be implemented in analog hardware. An alternative would be to employ a hexagonal grid, for which implementations already exist (e.g. [2,14]). But those would have to be extended to make them functioning with spiking units. One may try to emulate the resistive network with switched capacitors, which have been used for emulating dendritic processing [6,21]. Switched capacitors however, depend on a fast clock which is digital circuitry rendering the approach rather a mixed analog–digital implementation. Still, this seems to us the most promising starting point to develop a 2D map showing the here presented, required dynamics. There are however limitations to the possible range of dynamics that can be emulated with these switched-capacitor circuits, in particular slow dynamics are intricate to emulate. To alleviate that problem one would employ a speed pyramid.

4.2. Biological comparison

If the nervous system used such propagation maps for speed estimation, one may wonder where and how they might be emulated. With regard to the biophysical mechanism (the ‘how’ issue), we intend to firstly discuss the horizontal connection, in particular the subthreshold propagation through the horizontal connections. We see the following possibilities.

(1) The dense packing of dendrites may allow for a subthreshold propagation of activity through dendro-dendritic synapses.

(2) Neurons may be connected by gap junctions, which rapidly propagate charge. It was long believed that gap junctions hardly exist in neocortical neurons [23], yet recent studies have indeed found them in a neocortical network of electrically coupled inhibitory neurons [7,8]. It is therefore reasonable to assume that gap junctions may also exist between excitatory neurons but that they have not been identified yet.

(3) The extra-cellular matrix may also contribute to subthreshold wave propagation in some way. Several

studies have shown that rapid calcium waves can spread quickly through the gap-junctions of the glia network (e.g. [3]). These calcium waves can alter the extracellular calcium concentration rapidly and substantially, and could therefore have a significant effect on the electrical behavior of neurons. It was also pointed out by Koch that such extracellular dynamics are not well understood, yet worth to model [12].

We next discuss how different dynamics may be achieved in the biological substrate. We distinguish between the synaptic, the neuronal and the architectural level. On a synaptic level, one may possibly find different synaptic decay times. Indeed, the nervous system possesses a variety of excitatory and inhibitory synaptic dynamics [11]. For example, the α-amino-3-hydroxy-5-methylisoxazole-4-propionic acid (AMPA) synapse releases a post-synaptic current (PSC) of short duration (several milliseconds), the *N*-methyl-D-aspartate (NMDA) synapse releases a current of long-duration (several tens of milliseconds)—the latter however only after the membrane potential has already been elevated to a certain level. Inhibitory synapses, like the γ-aminobutyric acid (GABA), also come in variants with different dynamics. We regard this possibility however as too intricate to cover a range of speeds using only an interplay of such synaptic dynamics. On a neuronal level, different dynamics may be achieved with varying neuronal 'packing' densities in cortical layers. Would such variation in packing cause the large difference in the required dynamics? Possibly. Alternatively, evolution may have evolved a speed pyramid, which would be a solution on the architectural level. For instance, 'speed-neurons' in lower areas like the primary visual cortex, may fire for lower speeds, whereas higher areas may possess neurons firing for higher speeds. A thorough review of the experimental motion studies may bear hints on whether the visual system may use such a structure.

There is also the possibility that a mixture of different mechanisms is at work. It has already been suggested for the computation of direction and orientation selectivity (e.g. [12,25]), that not necessarily a mere, single mechanism solves this task, but a multitude of them working together. Similarly, that could be also the case for speed estimation.

Regarding the location of such maps (the 'where' issue), one may readily suggest that they exist in area MT (V5), where neurons seem to be involved in signaling speed (e.g. [15,16]). But the signal of MT speed-tuned neurons is also coupled to the direction of the moving grating. In contrast, in our system no direction selectivity is involved and these neurons are therefore 'purely' speed-tuned but such neurons have not been found yet. It may be that biological speed estimation is always related to direction computation. For example, we imagine that several coarse direction are computed in connection with several coarse speeds. To determine the exact direction and speed of a motion, the coarse tuning curves would be read out as suggested above.

The speed-tuning curves of the presented system resemble limitedly to the speed-tuning curves of MT cells. The latter are typically bell-shaped for a range of different speeds (e.g. [15,16]), whereas the former show only a bump-like shape for medium speeds. For fast and slow speeds, the speed-tuning curves are monotonically increasing and decreasing, respectively.

The system can potentially compute speed very swiftly because it uses single spikes only. The time it takes to signal speed depends on the integration time of the map. One may view this as a single spike code and such codes have already been suggested by others for instantaneous pattern recognition, i.e. [10,24].

5. Summary and outlook

A spiking propagation map was introduced that can detect the speed of motion input when its dynamics are properly tuned. The model can be regarded as an elaboration of Glaser and Barch's model [9] that includes now the introduction of a mechanism signaling speed. A crude simulation was run that outlines how such a map may fit into a neuromorphic architecture in which a silicon retina would provide the input to such propagation maps. The dynamics could be analyzed in more depth by using complex stimuli such as a pendulum stimulation (oscillation) or spiral-shaped motion input.

A next step in the elaboration of this model would be to include a mechanism of direction computation. This may require a sufficiently discerned look at the subject of motion detection. Motion detection may not be solvable with a single direction-selective mechanism but with different techniques for different specific motion inputs. A first step one may take is to perform tracking of a single object of limited size. To circumvent the aperture problem one may use large receptive fields that 'swallow' the entire object and that would therefore be insensitive to the exact contour orientations of the object. This may also bring the model closer to a possible comparison to neurophysiological findings.

With regard to a neuromorphic implementation, there are many technical issues that have to be addressed. Firstly, it requires the proper implementation of such a spiking propagation map, whereby the resistor issue may be the biggest hurdle to climb. Secondly, the actual use of a silicon retina as input may require substantial adjustment of the propagation map at the parameter level.

Acknowledgements

The study was carried out in Prof. Michael Wenger lab at the University of Notre Dame funded by a grant from the University Graduate School. The author wishes to thank Michael Wenger for generous support.

References

[1] H. Barlow, W. Levick, Mechanism of directly selective units in rabbits retina, J. Physiol. (London) 1 (1964) 477–504.

[2] K. Boahen, A retinomorphic chip with parallel pathways: encoding increasing, on, decreasing, and off visual signals, Analog Integr. Circuits Process. 30 (2) (2002) 121–135.
[3] A. Charles, Intercellular calcium waves in glia, Glia 24 (1) (1998) 39–49.
[4] R. Douglas, M. Mahowald, C. Mead, Neuromorphic analog VLSI, Ann. Rev. Neurosci. 18 (1995) 255–281.
[5] R. Douglas, C. Rasche, Silicon neurons, in: M.A., A. (Ed.), The Handbook of Brain Theory and Neural Networks, MIT Press, Cambridge, MA, 2002.
[6] J.G. Elias, Artificial dendritic trees, Neural Comput. 5 (1993) 648–664.
[7] M. Galarreta, S. Hestrin, A network of fast-spiking cells in the neocortex connected by electrical synapses, Nature 402 (6757) (1999) 72–75.
[8] J.R. Gibson, M. Beierlein, B.W. Connors, Two networks of electrically coupled inhibitory neurons in neocortex, Nature 402 (6757) (1999) 75–79.
[9] D. Glaser, D. Barch, Motion detection and characterization by an excitable membrane: the 'bow wave' model, Neurocomputing 26–27 (June) (1999) 137–146.
[10] J. Hopfield, Pattern recognition computation using action potential timing for stimulus representation, Nature 376 (1995) 33–36.
[11] D. Johnston, S. Wu, Foundations of Cellular Neurophysiology, MIT, Cambridge, MA, 1995.
[12] C. Koch, Computational Biophysics of Neurons, MIT, Cambridge, MA, 1999.
[13] M. Livingstone, Mechanisms of direction selectivity in macaque v1, Neuron 20 (3) (1998) 509–526.
[14] C.A. Mead, Analog VLSI and Neural Systems, Addison-Wesley, Reading, MA, 1989.
[15] J. Perrone, A. Thiele, Speed skills: measuring the visual speed analyzing properties of primate mt neurons, Nature Neurosci. 4 (5) (2001) 526–532.
[16] N. Priebe, C. Cassanello, S. Lisberger, The neural representation of speed in macaque area mt/v5, J. Neurosci. 23 (13) (2003) 5650–5661.
[17] W. Rall, Theoretical significance of dendritic trees for neuronal input–output relations, in: R. Reiss (Ed.), Neural Theory and Modelling, Stanford University Press, Stanford, 1964, pp. 73–97.
[18] C. Rasche, Signaling contours by neuromorphic wave propagation, Biol. Cybernet. 90 (4) (2004) 272–279.
[19] C. Rasche, Excitable maps for visual processing, 2005a, under review.
[20] C. Rasche, The Making of a Neuromorphic Visual System, Springer, New York, 2005b.
[21] C. Rasche, R. Douglas, Forward- and backpropagation in a silicon dendrite, IEEE Trans. Neural Networks 12 (2) (2001) 386–393.
[22] W. Reichardt, Autocorrelation, a principle for the evaluation of sensory information by the central nervous system, in: W. Rosenblith (Ed.), Sensory Communication, Wiley, New York, 1961, pp. 303–317.
[23] G. Shepard, The Synaptic Organization of the Brain, 4th ed., Oxford University Press, New York, NY, 1998.
[24] S.J. Thorpe, Spike arrival times: a highly efficient coding scheme for neural networks, in: R. Eckmiller, G. Hartmann, G. Hauske (Eds.), Parallel Processing in Neural Systems and Computers, Elsevier Science Publishers, Amsterdam, 1990, pp. 91–94.
[25] T. Vidyasagar, X. Pei, M. Volgushev, Multiple mechanisms underlying the orientation selectivity of visual cortical neurones, TINS 19 (1996) 272–2777.

Christoph Rasche received a diploma in theoretical neurobiology at the University of Zürich in 1996. He completed a Ph.D. degree in Computational Neuroscience, with a specialization in Neuromorphic Engineering, at the ETH Zürich in 1999. During a postdoctoral stay at Caltech, Pasadena, he began studying the subject of visual object representations. At UC Santa Barbara he started to acquire a background in visual psychophysics and currently continues to do so at Penn-State. His research interests are neuromorphic engineering of a visual recognition architecture, and visual perceptual learning.